PCCP

PAPER

Cite this: *Phys. Chem. Chem. Phys.*, 2018, **20**, 22730

Aggregation behavior of dihexadecylviologen bistriflimide ionic liquid crystal in different solvents: influence of polarity and concentration

Shen Li, [ab] Giacomo Saielli [*c] and Yanting Wang [*ab]

Received 14th May 2018,
Accepted 3rd August 2018

DOI: 10.1039/c8cp03055c

rsc.li/pccp

Solutions of 1,1′-dihexadecyl-4,4′-bipyridinium di[bis(trifluoromethanesulfonyl)imide] salt, also known as dihexadecylviologen bistriflimide, in deuterated acetonitrile (ACN), dichloromethane (DCM) and chloroform ($CDCl_3$), respectively, were investigated by the combination of ^1H and DOSY NMR spectroscopy, DFT calculations and MD simulation to understand the influence of solvent polarity and solute concentration (10^{-5}–10^{-1} M) on its aggregation behavior. We found that the polar solvent acetonitrile (ACN) does not favor ion aggregation and cluster formation. In the whole range of concentrations investigated, the system appears to be dominated by neutral ion pairs composed of one cation and two anions, possibly in fast equilibrium (on the NMR time scale) with small or slightly larger aggregates. The diffusion coefficient of the cationic species is only weakly affected by concentration. In contrast, the low-polar solvents of chloroform ($CDCl_3$) and dichloromethane (DCM) strongly favor cluster formation above a certain concentration and the viologen diffusion coefficient in $CDCl_3$ is much smaller and more strongly dependent on concentration than that in ACN. The information obtained from the MD simulations suggests that the aggregates have a structure similar to the isotropic liquid phase of the viologen-based ionic liquids and ionic liquid crystals. The lifetimes of such large clusters appear to be relatively long, beyond the time scale of tens of nanoseconds. Moreover, the results from the aromatic proton NMR resonances provide some insights on the dielectric constants inside the viologen aggregates.

Introduction

Viologen salts[1] have attracted a great deal of interest in recent years for their molecular redox and electrochromic properties[2,3] as well as their bulk behavior as ionic liquids (ILs)[4,5] and ionic liquid crystals (ILCs).[6–9] Their application as functional materials has also been recently reviewed.[10] The viologen unit is composed of a dialkylated bipyridinium core bearing two positive charges. The anions have a strong impact on bulk properties: for example, the melting point of viologen-based ILs is apparently influenced by the type of anions;[4,5] an even stronger effect is evident in the thermotropic behavior of viologen-based ILCs, whose ionic mesophases have their type and thermal range of stability determined by the anions. For example, while halide anions lead to high melting solid salts, their replacement with the hydrophobic, flexible and low-coordinating bistriflimide anions ($[Tf_2N]^-$) results in a rich mesomorphism with low-temperature IL and liquid-crystalline phases.[6–9]

Equally interesting is the behaviour of bistriflimide viologen salts in various solvents. The formation of various types of aggregates including micelles and vesicles has been studied, for example in combination with other surfactants, to impart the redox properties of the viologen to microemulsions[11] or for the production of stable Pt nanoparticles.[12] Recently, the use of viologen bistriflimide salts as additives in the fabrication of a highly fluorinated porous membrane for the production of desalted water was reported.[13] The viologen bistriflimide salt adsorbed on the membrane surface was intended to maintain a correct hydrophile/lipophile balance in order to improve the embedding action of the polymer constituting the membrane during the process in low-polar solvents like dichloromethane (DCM).[13] Therefore, it is very important to investigate the aggregation behavior of bistriflimide viologen salts in several solvents of different polarity and understand their behaviour as additives in the examples mentioned above.

This issue is part of a more general topic concerning the aggregation behaviour of ILs in various solvents. Several examples

[a] *CAS Key Laboratory of Theoretical Physics, Institute of Theoretical Physics, Chinese Academy of Sciences, 55 East Zhongguancun Road, P. O. Box 2735, Beijing, 100190, China. E-mail: wangyt@itp.ac.cn*
[b] *School of Physical Sciences, University of Chinese Academy of Sciences, 19A Yuquan Road, Beijing, 100049, China*
[c] *Istituto per la Tecnologia delle Membrane del CNR, Sezione di Padova, and Department of Chemical Sciences, University of Padova, Via Marzolo, 1, 35131 Padova, Italy. E-mail: giacomo.saielli@unipd.it*

can be found in the literature and critical reviews have been presented.[14,15] Such studies are often confined to polar solvents, often water,[16,17] because of the generally low solubility/miscibility of ionic systems with low or non-polar solvents. However, the behaviour of ILs and ILCs in low and non-polar solvents is very important in several instances. Hoffmann and co-workers recently investigated imidazolium ILs in low-polar solvents and found evidence of a bimodal distribution.[18] The details of these phenomena are still poorly understood,[19] nevertheless, in several cases, solutions of ILs in low-polar solvents have been used for practical purposes: besides the ones mentioned above, related with viologens, we can recall here liquid–liquid microextraction,[20] their use as co-solvents in chemical reactions[21] and morphological studies of polymeric membranes.[22]

Nuclear magnetic resonance (NMR) is a very powerful experimental technique for investigating the structural properties of molecules as well as supramolecular aggregates. In fact, proton resonances can also depend on intermolecular and solvent effects, and thus can be used as probes to detect the environmental structure surrounding a given probe solute.[23] However, the effect of the surrounding matrix is quite difficult to rationalize experimentally since it depends on the averaged structure and dynamics of the whole system. Therefore, computational methods based on density functional theory (DFT) calculations and/or molecular dynamics (MD) simulations are necessary to provide significant insights. Although DFT methods have proven to be extremely effective in predicting the NMR properties of organic molecules and natural products,[24–26] and also at a semiquantitative level of bulk ILs,[27,28] the extension of such protocols to supramolecular aggregates in solution, for which solvent effects, dynamics and weak intermolecular interactions play a dominant role, cannot be taken for granted. The opposite balance between pros and cons can be found in MD simulations: the method can fully account for the dynamics and the complexity of supramolecular aggregates in a given solvent, but minor details of the interactions responsible for the average structure of the system, and thus for the chemical shift of the active nuclei, cannot be exactly modelled by classical force fields (FFs). As an example, a significant improvement of the predicted average ^{1}H chemical shift of the ionic liquid 1-ethyl-3-methylimidazolium chloride was observed when DFT calculations were run on clusters extracted from an *ab initio* MD trajectory compared to that obtained using clusters extracted from a classical FF trajectory.[29]

In this work, we investigate the aggregation behaviour of dihexadecylviologen bistriflimide in deuterated acetonitrile, dichloromethane and chloroform by means of NMR spectroscopy, DFT calculation and MD simulation. The NMR experiments cover a relatively wide range of concentrations, from 10^{-5} up to 10^{-1} M. Moreover, diffusion coefficients of the cations have been measured by DOSY NMR experiments. Then, computational protocols are used to understand some features of the systems in the limit of low concentration (DFT) and to give a full description of the structural and dynamic properties of the systems in the limit of high concentration (MD).

Methods

Synthesis

For the synthesis of 1,1′-dihexadecyl-4,4′-bipyridinium di[bis(trifluoromethanesulfonyl)imide],[8,30] 500 mg of 4,4′-bipyridine (3.2 mmol) was refluxed with 2.15 mL (7.04 mmol) of 1-bromohexadecane in acetonitrile overnight. The yellow precipitate (1,1′-dihexadecyl-4,4′-bipyridinium dibromide) was filtered, washed with cold acetone and recrystallized from a 15 : 85 acetone : water mixture to finally obtain 2.0 g of product (yield 81%). The bromide salt was then dissolved in 20 mL of methanol and added to 20 mL of a methanol solution containing 1.1 excess of $LiTf_2N$ with respect to the bromide, and stirred for 4 h. The solvent was evaporated under vacuum and a white precipitate was formed after adding water to the flask. The white precipitate of dihexadecylviologen bistriflimide ($[C_{16}bpC_{16}][Tf_2N]_2$) was then filtered and washed with water until the removal of the halide ions (assay with an acidic solution of silver nitrate) and dried under vacuum in the presence of $CaCl_2$. Yield: 45%. ^{1}H NMR (MeOD, 500 MHz) δ = 9.24 (d, J = 6.7 Hz, 4H); 8.63 (d, J = 6.7 Hz, 4H); 4.73 (q, J = 7.6, 4H); 2.09 (broad, 4H); 1.43 (broad, 4H); 1.32–1.29 (broad, 48H); 0.90 (t, J = 6.7 Hz, 6H) ppm.

NMR spectroscopy

Solution-state NMR spectra of the ILs were collected with a Bruker AVANCE III spectrometer equipped with a 5 mm z-gradient broadband inverse (BBI) probe and operating at 500.13 MHz ^{1}H. Signals were referenced to tetramethylsilane (TMS) through the lock signal. Deuterated solvents, acetonitrile-d_3, dichloromethane-d_2 and chloroform-d_1, were purchased from SigmaAldrich. All experiments were run at 298 K.

^{1}H DOSY experiments were run with a Bruker AVANCE II HD 400 equipped with a 5 mm BBI z-grad probe (55.8 G/cm max gradient strength). Diffusion-ordered spectra were obtained by means of a stimulated-echo pulse sequence (STE) with bipolar gradient pulses (BPP) featuring an additional longitudinal eddy-current delay (LED).[31] Typical employed parameters were 1–2 ms for the encoding gradient length (δ), *ca.* 1000 ms for the diffusion delay (Δ) and 5 ms for the LED. Care was taken to quench possible temperature gradients (and the resulting convection) within the sample by increasing the refrigerating air flow to 800 L h^{-1}. Diffusion coefficients were estimated by fitting the experimental data to the model equation of ref. 31.

DFT calculation

Three different models were built to calculate the proton chemical shift using DFT protocols. The first model is represented by a single cation, the second one is a charged ion pair made by one cation along with one anion, and the third one is a neutral ion cluster made by one cation along with two anions. Structures were energetically minimized at the B3LYP/6-311G** level including the solvent reaction field by means of the PCM method[32] describing the solvent considered (either ACN, DCM or $CDCl_3$). The ^{1}H NMR isotropic shielding constant, σ, was then calculated using the optimized structures, still including the solvent reaction field, at the B3LYP/cc-pVTZ level.[24] Finally,

the chemical shift was obtained as $\sigma_{ref} - \sigma$, where σ_{ref} is the shielding constant of the reference, TMS, calculated at the same level of theory. All calculations were run with the software package Gaussian 09.[33]

As will be shown below, the diagnostic resonances come from the bipyridinium rings. Since we focused our attention on the electrostatic interaction between the anion and the aromatic charged viologen core, to save computer time, model systems for the DFT calculations were simplified to have a cation of $[C_2bpC_2]^{2+}$, which contains two ethyl chains instead of two hexadecyl chains.

MD simulation

Because MD simulations with periodic boundary conditions (PBCs) require the simulation box to be much larger than the molecular size, the long-chain cation of $[C_{16}bpC_{16}]^{2+}$ is difficult to model by MD simulation. Therefore, $[C_8bpC_8][Tf_2N]_2$ was used to run MD simulations since it shows a very similar aggregation behavior in low-polar solvents.[34] MD simulations were run for all three solvents investigated experimentally. We prepared a simulation box with 64 viologen ion pairs along with 6400 solvent molecules to keep a mole ratio of 1 : 100, corresponding to the high concentration range of about 0.1 mol L^{-1} in the experiments. Lower concentrations are difficult to simulate by MD since the simulation box would have to contain very few ions with vast amounts of solvent molecules, which would not only require a lot of computer time, but also would lead to poor statistics of solute molecules.

The force field parameters for $[C_8bpC_8]^{2+}$ and $[Tf_2N]^-$ were taken from the AMBER force field[35,36] and the partial charges were calculated with the RESP method.[37] The force field and the partial charges of all these solvents were taken from ref. 38 and 39, respectively. The PBCs were applied to all three dimensions of the cubic simulation box, and a 1.2 nm cutoff was applied to the non-bonded interactions. The particle mesh Ewald (PME)[40] method was employed to handle the long-range electrostatic interactions and the timestep was 1 fs. The temperature was controlled by the Nosé–Hoover thermostat[41] and the pressure for the preliminary *NPT* simulations was controlled by the Parrinello–Rahman barostat.[42] First, a 4 ns *NPT* MD simulation at $P = 1$ atm and $T = 300$ K was used to sample the average box size. The box sizes of the acetonitrile, dichloromethane and chloroform systems were found to be, on average, 8.86, 9.19 and 9.82 nm, respectively, corresponding to concentrations of 0.153, 0.123 and 0.112 mol L^{-1}, respectively, consistent with our experimental systems. An annealing procedure was then followed to cool the systems down from 1000 K to 300 K with a temperature interval of 100 K. At each temperature, a constant *NVT* MD simulation was run for 2 ns, amounting to a total pre-equilibration run of 16 ns. Finally, a 6 ns *NVT* MD simulation at $T = 300$ K was run to collect data with a sampling interval of 3 ps. The MD simulations were run with the GROMACS software package.[43]

Results

Experimental measurements

In Scheme 1, we show the structural formula of the viologen experimentally investigated by ^{1}H-NMR and DOSY spectroscopy.

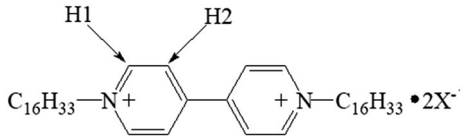

Scheme 1 Viologen salt ($[C_{16}bpC_{16}][Tf_2N]_2$) investigated in the NMR experiments ($X^- = (CF_3SO_2)_2N^-$).

The interesting resonances that can be used as probes of aggregation phenomena come from the aromatic protons labelled as H1 (the four protons in the *ortho* position with respect to the nitrogen atoms) and H2 (the four protons in the *meta* position with respect to the nitrogen atoms). H1 is usually the more de-shielded resonance compared to H2 due to the positively charged nitrogen. Nevertheless, the exact value in ppm strongly depends on the solvent and concentration. In contrast, all alkyl resonances of the alkyl chains are mostly unaffected by changing the solvent and/or concentration.

In Table 1, we report the dielectric constants of the solvents. Although we used deuterated solvents, the dielectric constant is almost identical to that of the non-deuterated analogue.[44] We can see that both dichloromethane and chloroform are low polar solvents while acetonitrile is a typical polar solvent with a dielectric constant of 35.7. At first glance, it seems surprising that an ionic system such as the viologen salt is highly soluble in low polar solvents. This can be understood by considering that both the cation and the anion considered are quite ''hydrophobic'' notwithstanding the fact that they are charged species, because the cation has two relatively long alkyl chains of 16 methylene groups and the negative charge of the anion is distributed over a relatively large surface leading to a very low coordinating ability.

When dissolved in acetonitrile at the lowest concentration investigated (see Fig. 1), the chemical shift δ of H1 and H2 is 8.91 and 8.39 ppm, respectively, and the relative shift is $\Delta\delta$ = 0.52 ppm. Increasing the concentration does not result in any appreciable effect: H1 and H2 resonances are 8.93 and 8.41 ppm, respectively, at the highest concentration investigated and the relative chemical shift still remains at $\Delta\delta$ = 0.52 ppm. Therefore, almost no concentration dependence is observed in the polar solvent acetonitrile.

In contrast, the chemical shift of H2 changes significantly with increasing concentration when dissolved in dichloromethane and chloroform. The variation of the H1 resonance is much smaller though still significant. When dissolved in dichloromethane, at the low-concentration limit, the H1 and H2 chemical shifts are 8.91 and 8.65 ppm, respectively, with a relative shift of 0.26 ppm. In particular, it appears that H2 is

Table 1 Dielectric constant ε of acetonitrile, dichloromethane, and chloroform

Solvent	ε
Acetonitrile	35.7
Dichloromethane	8.93
Chloroform	4.71

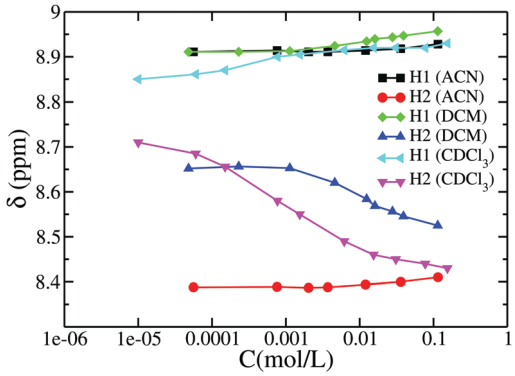

Fig. 1 Chemical shifts of H1 and H2 of the viologen salt dissolved in deuterated acetonitrile (ACN), dichloromethane (DCM), and chloroform ($CDCl_3$) at different concentrations.

de-shielded compared to acetonitrile while H1 is only slightly affected. In chloroform, the solvent studied with the lowest polarity, the chemical shifts of H1 and H2 are 8.85 and 8.71 ppm, respectively, in the limit of low concentration, with a relative shift of 0.14 ppm, even closer than those in dichloromethane.

With increasing concentration in the two low-polar solvents, the H1 chemical shift increases while the H2 chemical shift decreases, and the concentration dependence is relatively strong in the range of 10^{-3}–10^{-2} M. At the highest concentration investigated, the chemical shifts of H1 and H2 are 8.96 and 8.53 ppm, respectively, in dichloromethane (with an increased relative shift of 0.43 ppm), and 8.93 and 8.40 ppm in chloroform (with an increased relative shift of 0.53 ppm).

These trends clearly indicate that in the concentration range of 10^{-3}–10^{-2} M, strong cation–anion interactions lead to ion aggregation, which alters the chemical shifts of the aromatic core of the viologen. The concentration dependence of the chemical shifts weakens when the concentration is above 10^{-2} M. Since NMR can only detect averaged signals with respect to the characteristic molecular correlation time, the variation of chemical shift reflects the ensemble average of dynamically changed local structures. Therefore, it can be concluded that when dissolved in acetonitrile, the averaged local structure around H1 and H2 remains almost unchanged at various concentrations. In contrast, when dissolved in dichloromethane and chloroform, the averaged local structures around H1 and H2 gradually change with increasing concentration because of the aggregation phenomena.

To summarize, the proton H2 appears to be a much more sensitive probe of the environment than H1. Interestingly, in the low-concentration limit, the H2 resonance is de-shielded from *ca.* 8.4 ppm in the polar solvent ACN to *ca.* 8.7 ppm in the low-polar solvent chloroform. If the concentration is increased in chloroform up to the high concentration limit, the H2 resonance is again shielded until it takes a similar value to that at the low-concentration limit in ACN, which is around 8.3 ppm.

Diffusion coefficients of the solvent solutions of acetonitrile and chloroform, respectively, were also investigated by the DOSY NMR technique. Such experiments were limited to relatively high concentrations because of the lower sensitivity of the

Table 2 Experimental diffusion coefficients of the viologen cations and the solvent solutions of acetonitrile and chloroform

D (10^{-9} m^2 s^{-1})	Conc. (M)	Cation	Solvent
ACN	2.30×10^{-3}	1.10	5.1
	6.20×10^{-2}	0.86	4.1
$CDCl_3$	1.43×10^{-3}	0.44	2.1
	1.28×10^{-2}	0.27	2.4
	6.85×10^{-2}	0.14	2.4

DOSY experiment. The experimental data are reported in Table 2. In acetonitrile, the diffusion of cations is relatively fast (around 10^{-9} m^2 s^{-1}) and the dependence on the concentration is weak. When the concentration increases by more than an order of magnitude (from 2.3×10^{-3} M up to 6.2×10^{-2} M), the diffusion coefficient D only decreases by a factor of about 1.1/0.86 = 1.28, so it is very weakly dependent on the concentration. This suggests a poor aggregation of the viologen salt in acetonitrile. In contrast, the diffusion of cations in chloroform is about 1 order of magnitude slower than in acetonitrile, and it is relatively more strongly dependent on concentration: when the concentration rises from 1.4×10^{-3} M up to 6.8×10^{-2} M, the diffusion coefficient decreases by a factor of 4.4/1.4 = 3.14, much larger than for the case of acetonitrile. These results indicate that ion association in chloroform is stronger than in acetonitrile.

DFT calculations

In order to understand the ^{1}H NMR results, we calculated by DFT methods the chemical shift of some selected optimized supramolecular structures including a single cation, a charged 1 : 1 cation–anion pair, and a neutral 1 : 2 cluster. Since it is impractical to calculate chemical shifts for relatively large clusters, we provide some insights into the NMR results by utilizing these simplified models. The rationale behind these types of calculations is that due to the extreme sensitivity of NMR to molecular structure and also to environmental effects, an agreement between the calculated and experimental values would suggest that the model structure used for the calculation is representative of the average structure in solution. We ran DFT calculations for these three solvents and the results are reported in Table 3.

Table 3 shows that the chemical shifts of H1 and H2 on a single cation in acetonitrile calculated by DFT are 8.97 and 8.47 ppm, respectively. Even though this model is quite simplified,

Table 3 The chemical shifts of model systems made of one cation, one cation with one anion, and one cation with two anions, calculated with DFT-PCM (solvent is ACN, DCM and $CDCl_3$)

	$CDCl_3$		DCM		ACN	
δ, ppm	H1	H2	H1	H2	H1	H2
C_2bpC_2	9.00	8.43	8.98	8.45	8.97	8.47
$C_2bpC_2{\cdot}Tf_2N$	8.78	8.68	8.82	8.62	8.84	8.58
$C_2bpC_2{\cdot}(Tf_2N)_2$	9.12	8.61	9.15	8.60	9.46	9.67

the result is still in very good agreement with the experimental data of 8.91 ~ 8.93 (H1) and 8.39 ~ 8.41 (H2) ppm (see Fig. 1). Thus, it can be inferred that when dissolved in acetonitrile, the association or interaction between the viologen bipyridinium ring and the Tf_2N^- anion is very weak at various concentrations. The majority of ions likely exist in the form of free ions or ion pairs and the lifetime of possible small aggregates, if they exist, should be rather short on the NMR time scale.

On the other hand, as shown in Table 3, the DFT results for the 1 : 1 and 1 : 2 aggregates poorly correlate with the experimental data, except for a qualitative agreement between the calculated 1 : 1 cluster and the experimental value in the low-concentration limit in chloroform and dichloromethane. This seems to indicate that in the low-concentration limit, stable and long-lived aggregates are formed in low polar solvents. However, the results for the neutral cluster are not quantitatively comparable with experiments and more importantly, while DFT can give some hints on the structures present in the low-concentration limit, it cannot say anything for a high concentration, since in that case, the full dynamics of the system needs to be taken into account, and it is impractical to run DFT calculations for clusters with a relatively large size.

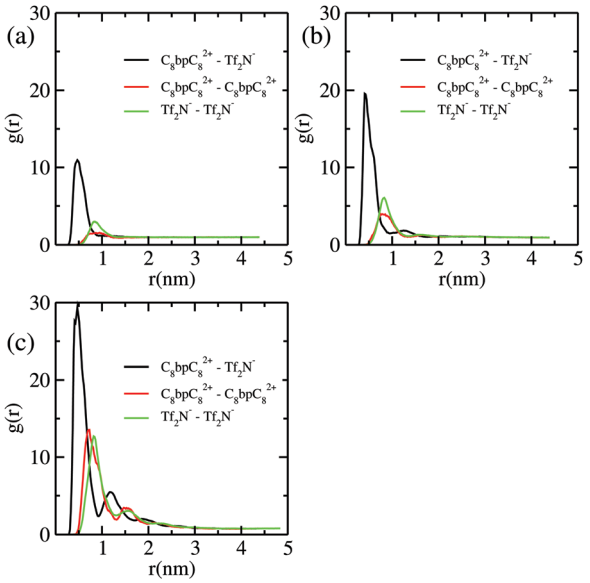

Fig. 3 RDFs of cation–anion (black line), cation–cation (red line), and anion–anion (green line) for the salt dissolved in ACN (a), DCM (b) and $CDCl_3$ (c). The geometric centres of cations and anions are used in the calculations of the distance.

MD simulations

We also ran MD simulations to gain a better understanding of the high-concentration behaviour of the viologen salt in these three solvents. Fig. 2 shows the snapshots of the MD simulations of the viologen salt dissolved in acetonitrile, dichloromethane and chloroform, respectively (solvent is omitted for clarity). Even a simple visual inspection reveals a very different degree of aggregation in these solvents. For a more quantitative analysis, the following properties were obtained from the MD trajectories: structural properties including the radial distribution function (RDF) and the spatial distribution function (SDF) and dynamic properties including the mean squared displacement (MSD) and the residence-time correlation function (RTCF).

In Fig. 3, we show the RDFs for the geometric centre of cations and anions dissolved in all these three solvents. We can see from Fig. 3a that the RDFs for ions in acetonitrile only exhibit a single less aggregated peak, indicating that both cations and anions are almost homogeneously distributed in solution. In contrast, Fig. 3c shows that the RDFs for ions in chloroform are more structured with three peaks, indicating that cations and anions are more aggregated when dissolved in chloroform. Fig. 3b shows that when dissolved in dichloromethane, the degree of aggregation is intermediate and closer to that observed in chloroform.

In Fig. 4, we report the SDFs of anions around cations for the salt in acetonitrile and chloroform, respectively, to visualize its aggregation behavior. The SDFs for the salt in dichloromethane are not present since the corresponding RDFs reveal that the aggregation behaviour in dichloromethane is qualitatively similar to the case of chloroform. When dissolved in acetonitrile at a high concentration, only one isosurface of maximum probability can be observed. It is roughly cylindrically distributed around the bipyridinium core, while no evidence of interaction

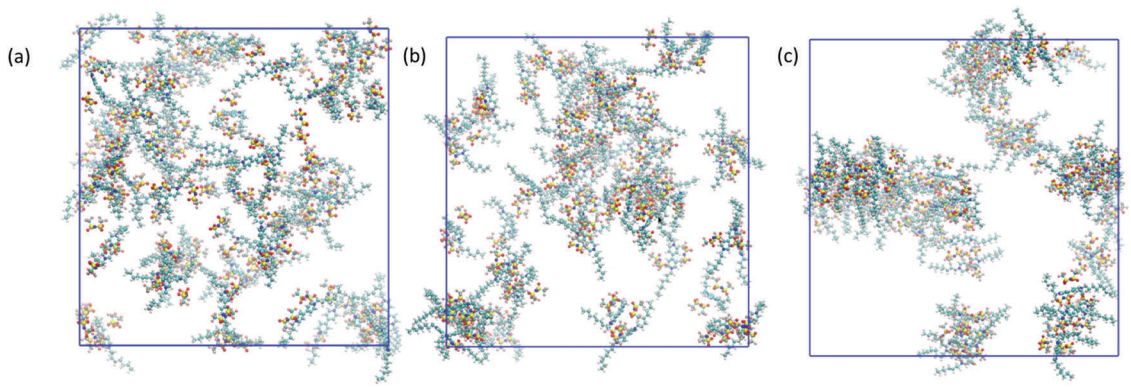

Fig. 2 Snapshots from the MD simulations of the viologen salt dissolved in acetonitrile (a), dichloromethane (b) and chloroform (c). Only cations ($[C_8bpC_8^{2+}]$) and anions ($[Tf_2N^-]_2$) are represented.

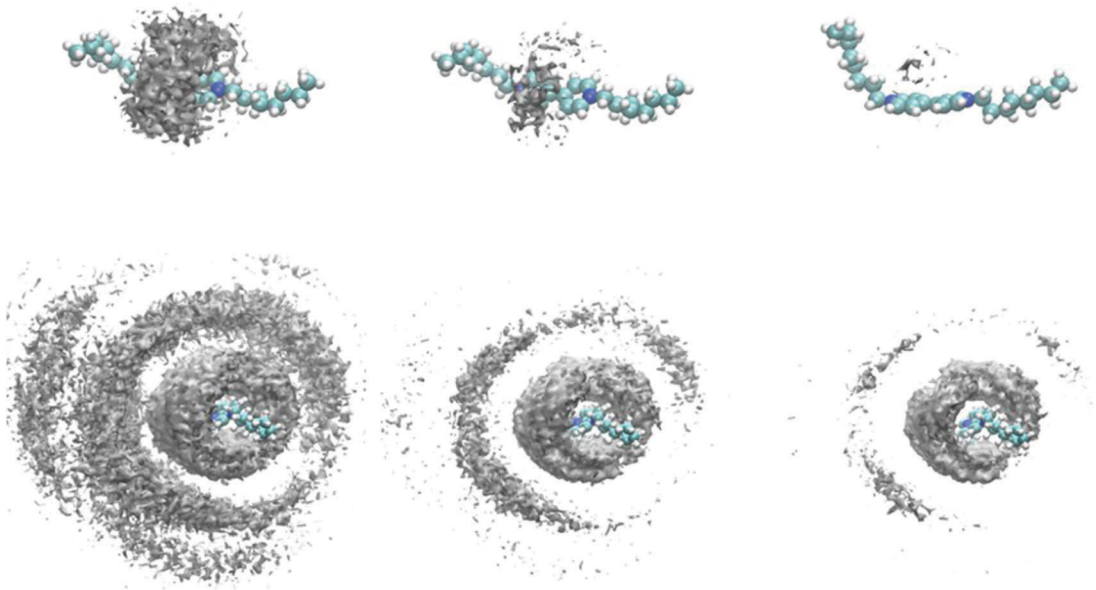

Fig. 4 Spatial distributions of anions ($[Tf_2N^-]_2$) around cations ($[C_8bpC_8^{2+}]$) for the salt dissolved in acetonitrile (top) and chloroform (bottom). The isosurface value increases from left to right, first column = 50, second column = 70, and third column = 90. The mean density of the system isovalue is about 40.

between the anions and the alkyl chains is observed, which also validates the choice of octylviologen, in the MD simulations, as a model system for hexadecylviologen. With an isosurface value of 40 for the mean bulk density, the isosurface is quickly reduced in size as the isocontour value increases to 70. Finally, there is almost no isosurface when the contour value increases up to 90, just above twice the mean bulk density of the ion pairs. In contrast, when dissolved in chloroform at high concentrations, the spatial distribution of the anions can clearly form two complete layers around the bipyridinium core, and a third one is also visible.

All these structural results suggest that the ions are aggregated and the clusters are relatively large and stable when dissolved in chloroform at high concentrations, while the aggregation appears to be very limited when dissolved in acetonitrile.

It is also quite instructive to investigate the dynamic properties of the two systems. Fig. 5a shows the MSDs of cations and anions dissolved in acetonitrile, dichloromethane and chloroform.

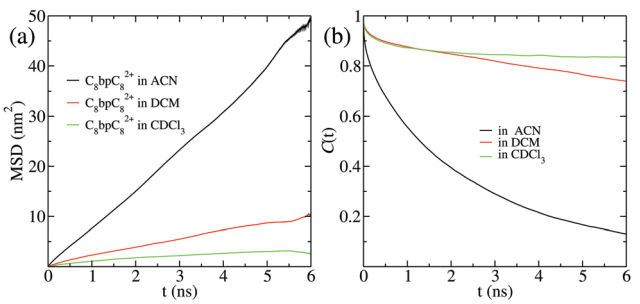

Fig. 5 (a) MSDs of cations dissolved in acetonitrile, dichloromethane and chloroform. (b) The RTCFs for the viologen salts dissolved in acetonitrile, dichloromethane and chloroform.

Table 4 Diffusion coefficients of the cation, anion, and solvent molecule in ACN, DCM and $CDCl_3$, respectively

D (10^{-9} m s^{-2})	ACN	DCM	$CDCl_3$
Cation	1.32(0.15)	0.27(0.01)	0.08(0.03)
Anion	1.40(0.18)	0.26(0.02)	0.07(0.03)
Solvent	6.68(0.03)	2.84(0.01)	1.98(0.05)

We can clearly see that the MSD slope for the cations in acetonitrile is much larger than in dichloromethane, which is somewhat larger than in chloroform. The corresponding self-diffusion coefficients (see Table 4) of ions as well as solvent molecules were determined by a linear fit of the MSDs using the Einstein relation $\langle \Delta r(t)^2 \rangle = 6Dt$. In acetonitrile, the self-diffusion coefficients of cations and anions are very close and about 5 times smaller than that of the acetonitrile molecules. In dichloromethane, they are also very close and about 10 times smaller than that of the dichloromethane molecules. In chloroform, they are again quite similar and about 25 times smaller than the diffusion coefficient of chloroform molecules. All these results indicate that the diffusion coefficients of cations and anions do not simply scale with the viscosity of all these solvents: they are about 20 times smaller when dissolved in chloroform than in acetonitrile due to ion clustering in chloroform. The diffusion coefficients that we obtained from MD simulations are fully consistent with the data obtained experimentally, although measured at slightly different concentrations. Nevertheless, we observed both from MD and DOSY experiments that ACN has a two–three times higher diffusion coefficient than $CDCl_3$ and that the diffusion of the viologen cations is about one order of magnitude faster in ACN with respect to $CDCl_3$.

Finally, in Fig. 5(b), we show the residence time correlation function (RTCF). The RTCF is defined as $C(t) = \langle p(0)p(t) \rangle$, where

$p(t)$ equals 1 if a given ion is still in the same ion shell (defined by the first minimum of the RDF) at time t or 0 otherwise; this function can be used to characterize the lifetime of the aggregates. It appears that when dissolved in acetonitrile, the lifetime of ion pairs decreases gradually and becomes lower than 0.2 after 6 ns. Note that this is a short time compared to the NMR time scale, which is generally in the range of micro- to milli-seconds. By contrast, when dissolved in dichloromethane and chloroform, its decay is very slow and beyond the possibility of being accurately determined within the 6 ns production run of the MD simulations; this result clearly highlights that ion clusters are formed and remain stable for a relatively long time when dissolved in chloroform at high concentrations.

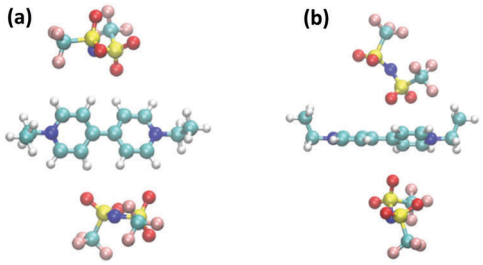

Fig. 6 Geometries selected for the model DFT calculations at a distance of 0.5 nm. Fixed atoms as the geometry center and the distance between cations and anions are shown. Panel (a) shows anions on the right and left sides of the aromatic rings, and panel (b) shows anions on the top and bottom of the aromatic rings.

Discussion

A detailed quantitative understanding of the chemical-shift dependence on viologen concentration and solvent polarity would require an averaged result of DFT calculations on clusters whose configurations are extracted from the MD trajectory. Although this approach has been successfully used to rationalize, for example, the NMR properties of ^{129}Xe dissolved in different ionic liquids,[45] its application to the present case would require considering very large clusters of molecules (in contrast to a Xe atom within its first solvation shell) making the calculation impractical. However, some qualitative issues can be discussed based on our current DFT calculation and MD simulation results. The RDFs and SDFs clearly indicate that the anions are arranged preferentially around the bipyridinium core and the maximum of probability is at the geometric centre of the bipyridinium. This might explain why the resonance of H2 protons is more sensitive to solvent polarity and concentration than H1. The closer proximity to the anions as the concentration is increased (similar effect as the polarity is decreased since less polar solvents favour tighter ion pairs) makes the H2 protons more sensitive probes of the environment. To test this point, we ran additional DFT calculations using fixed geometries of the neutral ion pair: anions were placed on symmetric points with respect to the bipyridinium core of the C_2bpC_2 model, both on the top and bottom of the aromatic rings, as well as on their sides, as in Fig. 6, an arrangement which is suggested by the SDFs shown in Fig. 4.

The geometric centres (see Fig. 6) of one cation and two anions were then symmetrically fixed at the distances of 0.5, 1.0, 1.5 and 2.0 nm, respectively, to calculate the chemical shifts by DFT calculation at the same level of theory used above, and the values of equivalent protons were averaged. The calculated values are reported in Fig. 7. We can see that the chemical shift of the H1 protons remains relatively constant as a function of the distance between the viologen core and the anions: there is only a slight decrease with increasing distance. By contrast, the chemical shift of the H2 protons is more sensitive: it decreases sharply before remaining constant with increasing distance when the distance between the viologen core and the anions is larger than 1 nm.

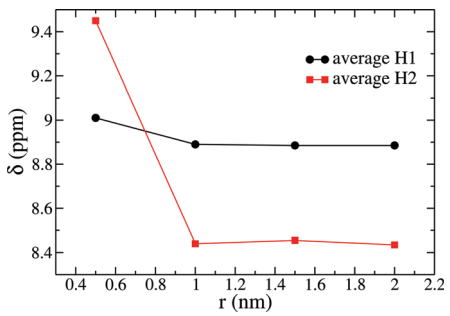

Fig. 7 The calculated chemical shifts of H1 and H2 as a function of the distance for the fixed-geometry models.

Moreover, the DFT results obtained using this simple model system suggest that the H2 protons are more de-shielded, and thus their chemical shift is increased when the anions are closer to the bipyridinium cation, while the chemical shift of the H1 protons is only slightly affected. The results of the experiments (Fig. 1), or at least the most qualitatively significant ones, can be summarized as follows: (i) in the low-concentration limit, lowering the polarity of the solvent largely de-shields the H2 resonance, which changes from *ca.* 8.4 ppm in ACN up to more than 8.7 ppm in chloroform, while the H1 resonance is only very slightly shielded; (ii) increasing the concentration in the low-polar solvent chloroform largely shields the H2 resonance, which goes from more than 8.7 ppm at the low-concentration limit back to *ca.* 8.4 ppm at high concentrations, while the H1 resonance is only slightly de-shielded, and both resonances are unaffected in polar solvents.

We can reconcile the experimental observations and the DFT results by considering the following: (i) lowering the polarity in the low-concentration limit indeed favours tighter binding of ion pairs: the effect of a higher dielectric constant in polar solvents weakens the electrostatic interaction, so in low-polar solvents such as chloroform, ion-pairs are expected to have a stronger interaction, keeping ions closer, which leads to shielding of the H2 resonance in the low-concentration limit when changing the solvent from high-polar ACN to low-polar chloroform; (ii) in the low-polar solvent, increasing the concentration leads to the formation of clusters, but inside the clusters,

ion pairs between viologen cations and bistriflimide anions are again less tightly bound than the single ion pair observed at the low-concentration limit. This can be understood by considering that the dielectric constant of ionic liquids is in the range of 10–30,[46] significantly larger than chloroform. Therefore, bipyridinium cations buried inside large viologen bistriflimide aggregates experience an average dielectric constant much larger than the one experienced by the single ion pair in the low-concentration limit and, as a consequence, a larger contact distance. The overall result is that the chemical shift in the low-polar solvent at high concentrations tends to have similar values to those observed in the polar solvent at all concentrations, since the dielectric constant is relatively large in both cases, in ACN solvent and inside the aggregates.

To summarize, the dependence of the chemical shift of the viologen protons on both polarity and concentration is actually mostly determined by the average distance between anions and bipyridinium, which is strongly modulated by the dielectric constant of the medium, since they are charged species essentially interacting through Coulombic attraction. In turn, the dielectric constant changes with the solvent but also, apparently, with the aggregation state of the viologen salt.

Conclusions

In this study, NMR experiments, DFT calculations, and MD simulations have been used to investigate the aggregation behavior of a viologen bistriflimide salt in various solvents. The results indicate that both solvent polarity and concentration have a strong influence on the behavior of the systems. In polar solvents like acetonitrile, ion aggregation forming large clusters is disfavored, and only small clusters can be formed with a relatively short lifetime. By contrast, when dissolved in nonpolar solvents, such as dichloromethane (DCM) and chloroform ($CDCl_3$), viologen ions form large aggregates with a relatively long lifetime of more than several tens of nanoseconds. The aromatic protons, especially those in the *meta* position with respect to the nitrogen of the pyridinium ring, are very sensitive probes of the environment and the trend of their chemical-shift change with solvent polarity and concentration can be qualitatively rationalized as a result of the average cation–anion distance: a closer ion distance leads to a more de-shielded proton resonance. The average distance is determined mainly by the effective dielectric constant of the medium screening the electrostatic interaction. Ion pairs are in closer contact in low-polar solvents because the Coulomb attraction between ions is less screened, while they have a larger average distance both in polar solvents and aggregates formed in a low-polar solvent at high concentrations. In both cases, the resonance of the *meta* protons is more shielded.

Conflicts of interest

There are no conflicts to declare.

Acknowledgements

This work was supported by the National Natural Science Foundation of China (No. 11774357 and 11747601) and the CAS Biophysics Interdisciplinary Innovation Team Project (No. 2060299). We thank the CNR-CAS bilateral agreement 2014-2016 for sponsoring a visit of S. L. to Padova and the CNR-CAS bilateral agreement 2017–2019 for financial support. G. S. also thanks the CAS President's International Fellowship Initiative (No. 2017VMC0005). Finally, we thank the Department of Chemical Sciences of the University of Padova for the allocation of computer time on the Linux clusters of the C3P community and for the allocation of time on the NMR instruments. We thank Dr I. Menegazzo for help with the NMR DOSY experiments. The allocations of computer time on Tianhe-2 supercomputer and the HPC Cluster of ITP-CAS are also appreciated.

Notes and references

1 P. M. S. Monk, *The viologens*, Wiley, Chichester, UK, 1999.
2 P. M. S. Monk and N. M. Hodgkinson, *Electrochim. Acta*, 1998, **43**, 245–255.
3 T.-H. Chang, H.-C. Lu, M.-H. Lee, S.-Y. Kao and K.-C. Ho, *Sol. Energy Mater. Sol. Cells*, 2018, **177**, 75–81.
4 N. Jordao, H. Cruz, A. Branco, C. Pinheiro, F. Pina and L. C. Branco, *RSC Adv.*, 2015, **5**, 27867–27873.
5 N. Jordao, L. Cabrita, F. Pina and L. C. Branco, *Chem. – Eur. J.*, 2014, **20**, 3982–3988.
6 K. Tanabe, T. Yasuda, M. Yoshio and T. Kato, *Org. Lett.*, 2007, **9**, 4271–4274.
7 G. Casella, V. Causin, F. Rastrelli and G. Saielli, *Liq. Cryst.*, 2016, **43**, 1161–1173.
8 G. Casella, V. Causin, F. Rastrelli and G. Saielli, *Phys. Chem. Chem. Phys.*, 2014, **16**, 5048–5051.
9 P. K. Bhowmik, S. T. Killarney, J. R. A. Li, J. J. Koh, H. Han, L. Sharpnack, D. M. Agra-Kooijman, M. R. Fisch and S. Kumar, *Liq. Cryst.*, 2017, **11**, 1–14.
10 L. Striepe and T. Baumgartner, *Chem. – Eur. J.*, 2017, **23**, 16924–16940.
11 J. H. Mondal, S. Ahmed and D. Das, *Langmuir*, 2014, **30**, 8290–8299.
12 G. Q. Gao, L. Lin, C. M. Fan, Q. Zhu, R. X. Wang and A. W. Xu, *J. Mater. Chem. A*, 2013, **1**, 12206–12212.
13 M. L. Perrotta, G. Saielli, G. Casella, F. Macedonio, L. Giorno, E. Drioli and A. Gugliuzza, *Appl. Mater. Today*, 2017, **9**, 1–9.
14 T. L. Greaves and C. J. Drummond, *Chem. Soc. Rev.*, 2008, **37**, 1709–1726.
15 H. K. Stassen, R. Ludwig, A. Wulf and J. Dupont, *Chem. – Eur. J.*, 2015, **21**, 8324–8335.
16 J. Bowers, C. P. Butts, P. J. Martin, M. C. Vergara-Gutierrez and R. K. Heenan, *Langmuir*, 2004, **20**, 2191–2198.
17 O. Naderi and R. Sadeghi, *J. Chem. Thermodyn.*, 2016, **102**, 68–78.

18 E. A. Cade, J. Petenuci and M. M. Hoffmann, *ChemPhysChem*, 2016, **17**, 520–529.
19 Y. P. Jiang, H. Nadolny, S. Kashammer, S. Weibels, W. Schroer and H. Weingartner, *Faraday Discuss.*, 2012, **154**, 391–407.
20 R. P. Monasterio and R. G. Wuilloud, *J. Anal. At. Spectrom.*, 2010, **25**, 1485–1490.
21 N. D. Khupse and A. Kumar, *J. Phys. Chem. A*, 2011, **115**, 10211–10217.
22 G. E. Romanos, O. C. Vangeli, K. L. Stefanopoulos, E. P. Kouvelos, S. K. Papageorgiou, E. P. Favvas and N. K. Kanellopoulos, *Microporous Mesoporous Mater.*, 2009, **120**, 53–61.
23 A. Bagno, F. Rastrelli and G. Saielli, *Prog. Nucl. Magn. Reson. Spectrosc.*, 2005, **47**, 41–93.
24 A. Bagno and G. Saielli, *Wiley Interdiscip. Rev.: Comput. Mol. Sci.*, 2015, **5**, 228–240.
25 A. M. Sarotti, *Org. Biomol. Chem.*, 2013, **11**, 4847–4859.
26 S. G. Smith and J. M. Goodman, *J. Am. Chem. Soc.*, 2010, **132**, 12946–12959.
27 V. P. Swamy, H. V. Thulasiram, F. Rastrelli and G. Saielli, *Phys. Chem. Chem. Phys.*, 2018, **20**, 11470–11480.
28 S. Chen and E. I. Izgorodina, *Phys. Chem. Chem. Phys.*, 2017, **19**, 17411–17425.
29 A. Bagno, F. D'Amico and G. Saielli, *ChemPhysChem*, 2007, **8**, 873–881.
30 P. K. Bhowmik, H. S. Han, J. J. Cebe, R. A. Burchett, B. Acharya and S. Kumar, *Liq. Cryst.*, 2003, **30**, 1433–1440.
31 D. H. Wu, A. D. Chen and C. S. Johnson, *J. Magn. Reson., Ser. A*, 1995, **115**, 260–264.
32 G. Scalmani and M. J. Frisch, *J. Chem. Phys.*, 2010, **132**, 15.
33 G. W. Trucks, M. J. Frisch, H. B. Schlegel, G. E. Scuseria, M. A. Robb, J. R. Cheeseman, G. Scalmani, V. Barone, B. Mennucci, G. A. Petersson, H. Nakatsuji, M. Caricato, X. Li, H. P. Hratchian, A. F. Izmaylov, J. Bloino, G. Zheng, J. L. Sonnenberg, M. Hada, M. Ehara, K. Toyota, R. Fukuda, J. Hasegawa, M. Ishida, T. Nakajima, Y. Honda, O. Kitao, H. Nakai, T. Vreven, J. A. Montgomery, Jr., J. E. Peralta, F. Ogliaro, M. Bearpark, J. J. Heyd, E. Brothers, K. N. Kudin, V. N. Staroverov, R. Kobayashi, J. Normand, K. Raghavachari, A. Rendell, J. C. Burant, S. S. Iyengar, J. Tomasi, M. Cossi, N. Rega, J. M. Millam, M. Klene, J. E. Knox, J. B. Cross, V. Bakken, C. Adamo, J. Jaramillo, R. Gomperts, R. E. Stratmann, O. Yazyev, A. J. Austin, R. Cammi, C. Pomelli, J. W. Ochterski, R. L. Martin, K. Morokuma, V. G. Zakrzewski, G. A. Voth, P. Salvador, J. J. Dannenberg, S. Dapprich, A. D. Daniels, Ö. Farkas, J. B. Foresman, J. V. Ortiz, J. Cioslowski and D. J. Fox, *Gaussian 09*, Gaussian, Inc., Wallingford, CT, 2009.
34 E. Marotta, F. Rastrelli and G. Saielli, *J. Phys. Chem. B*, 2008, **112**, 16566–16574.
35 J. M. Wang, R. M. Wolf, J. W. Caldwell, P. A. Kollman and D. A. Case, *J. Comput. Chem.*, 2004, **25**, 1157–1174.
36 W. D. Cornell, P. Cieplak, C. I. Bayly, I. R. Gould, K. M. Merz, D. M. Ferguson, D. C. Spellmeyer, T. Fox, J. W. Caldwell and P. A. Kollman, *J. Am. Chem. Soc.*, 1995, **117**, 5179–5197.
37 R. J. Woods and R. Chappelle, *J. Mol. Struct.: THEOCHEM*, 2000, **527**, 149–156.
38 A. M. Nikitin and A. P. Lyubartsev, *J. Comput. Chem.*, 2007, **28**, 2020–2026.
39 T. Fox and P. A. Kollman, *J. Phys. Chem. B*, 1998, **102**, 8070–8079.
40 U. Essmann, L. Perera, M. L. Berkowitz, T. Darden, H. Lee and L. G. Pedersen, *J. Chem. Phys.*, 1995, **103**, 8577–8593.
41 W. G. Hoover, *Phys. Rev. A: At., Mol., Opt. Phys.*, 1985, **31**, 1695–1697.
42 M. Parrinello and A. Rahman, *J. Appl. Phys.*, 1981, **52**, 7182–7190.
43 H. J. C. Berendsen, D. Vanderspoel and R. Vandrunen, *Comput. Phys. Commun.*, 1995, **91**, 43–56.
44 J. Wyman and E. N. Ingalls, *J. Am. Chem. Soc.*, 1938, **60**, 1182–1184.
45 G. Saielli, A. Bagno, F. Castiglione, R. Simonutti, M. Mauri and A. Mele, *J. Phys. Chem. B*, 2014, **118**, 13963–13968.
46 T. Singh and A. Kumar, *J. Phys. Chem. B*, 2008, **112**, 12968–12972.

